RKKY interaction in one-dimensional flat band lattices

Katharina Laubscher,[1] Clara S. Weber,[2,3] Maximilian Hünenberger,[1] Herbert Schoeller,[2] Dante M. Kennes,[2,4] Daniel Loss,[1] and Jelena Klinovaja[1]

[1] *Department of Physics, University of Basel, Klingelbergstrasse 82, CH-4056 Basel, Switzerland*
[2] *Institut für Theorie der Statistischen Physik, RWTH Aachen, 52056 Aachen, Germany and JARA - Fundamentals of Future Information Technology*
[3] *Department of Physics and Astronomy, University of Pennsylvania, Philadelphia, Pennsylvania 19104, USA*
[4] *Max Planck Institute for the Structure and Dynamics of Matter, Center for Free Electron Laser Science, 22761 Hamburg, Germany*

(Dated: October 19, 2022)

We study the Ruderman-Kittel-Kasuya-Yosida (RKKY) interaction between two classical magnetic impurities in one-dimensional lattice models with flat bands. As two representative examples, we pick the stub lattice and the diamond lattice at half filling. We first calculate the exact RKKY interaction numerically and then compare our data to results obtained via different analytical techniques. In both our examples, we find that the RKKY interaction exhibits peculiar features that can directly be traced back to the presence of a flat band. Importantly, these features are not captured by the conventional RKKY approximation based on non-degenerate perturbation theory. Instead, we find that degenerate perturbation theory correctly reproduces our exact results if there is an energy gap between the flat and the dispersive bands, while a non-perturbative approach becomes necessary in the absence of a gap.

Introduction. Magnetic impurities embedded in a host material can interact indirectly by coupling to the electron spin density of the host. This so-called Ruderman-Kittel-Kasuya-Yosida (RKKY) interaction [1–3] can result in a magnetic ordering of the impurity spins, leading to a wide range of interesting phenomena with potential applications in the fields of spintronics [4, 5], spin-based quantum computation [6–10], or engineered topological superconductivity [13–23]. The exact form of the RKKY interaction depends on the properties—in particular, the band structure—of the underlying host material and has been extensively studied for various types of systems [24–55].

Conventionally, the RKKY interaction is calculated in second-order perturbation theory assuming that the exchange coupling between the impurity spins and the itinerant electrons is small compared to the typical energy scale of the latter. Recently, however, systems with so-called *flat bands* have attracted significant attention [56, 57]. The energy of these bands is completely independent of momentum or, in a weaker sense, at least approximately constant over a large range of allowed momenta. While the recent interest in flat-band systems has mainly been fueled by significant theoretical and experimental progress on Moiré materials such as twisted bilayer graphene [58–63], flat bands can also emerge as Landau levels in two-dimensional electron gases subjected to a strong magnetic field or in a variety of artificial lattice models [64, 65], some of which have successfully been realized in experiments using photonic lattices or cold-atom setups [66–71].

In this case, the vanishing band width and the large degeneracy of the flat band make it questionable whether the conventional perturbative approach to the RKKY interaction is still applicable. This issue was first touched upon in the context of zigzag graphene nanoribbons, where exact numerical studies of edge impurities revealed unconventional features of the RKKY interaction that had not been captured by preceding analytical studies [35, 72]. Later, Ref. [73] studied the RKKY interaction in partially filled graphene Landau levels using *degererate* perturbation theory. On the other hand, a few more recent studies calculate the RKKY interaction in flat-band lattice models via standard non-degenerate

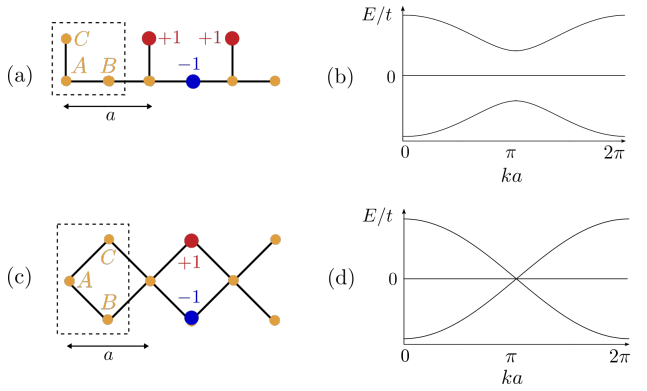

FIG. 1. (a) Stub lattice. The unit cell (dashed rectangle) consist of three sites (orange dots) labeled A, B, and C. Nearest-neighbor sites are connected by a hopping term of strength t (black lines). The flat band is spanned by a set of CLSs that has support on only three lattice sites each (red and blue dots). The amplitudes of the unnormalized CLSs are $+1$ (-1) for the red (blue) sites. (b) Bulk spectrum of the stub lattice. The dispersive bands are separated from the flat band by an energy gap. (c) Diamond lattice. The graphical elements have the same meaning as in panel (a). Here, the CLSs spanning the flat band have support on only two lattice sites each. (d) Bulk spectrum of the diamond lattice. The dispersive bands touch the flat band in a linear band touching point.

perturbation theory [74, 75]. As such, it becomes evident that a general understanding of RKKY effects in flat-band systems—including, in particular, insights regarding the applicability and limitations of perturbation theory—is still lacking. With this motivation, we carefully study the RKKY interaction in two simple one-dimensional (1D) flat-band systems at half filling, see Fig. 1. We first calculate the exact RKKY interaction numerically and then compare our data to results obtained via different analytical techniques. In both our examples, we find that the RKKY interaction exhibits peculiar features that are not captured by the conventional RKKY approximation based on non-degenerate perturbation theory. Instead, we find that degenerate perturbation theory correctly reproduces our exact results if there is an energy gap between the flat and the dispersive bands, while a non-perturbative approach becomes necessary in the absence of a gap.

Models. Let us start by introducing the stub lattice, see Fig. 1(a). A unit cell consists of three sites labeled A, B, and C. Neighboring sites are coupled by a hopping element of strength t, such that

$$H_{\text{stub}} = t\sum_n \left(c^\dagger_{n,A}c_{n,B} + c^\dagger_{n,C}c_{n,B} + c^\dagger_{n+1,B}c_{n,A}\right) + \text{H.c.} \tag{1}$$

Here, $c^\dagger_{n,l}$ ($c_{n,l}$) creates (destroys) a spinless electron on sublattice $l \in \{A, B, C\}$ in the nth unit cell. Imposing periodic boundary conditions on a chain with a finite number of unit cells N, the Hamiltonian can be rewritten in momentum space as $H_{\text{stub}} = \sum_k \Psi^\dagger_k \mathcal{H}(k)\Psi_k$ with $\Psi_k = (c_{k,A}, c_{k,B}, c_{k,C})^T$ and

$$\mathcal{H}(k) = t\begin{pmatrix} 0 & 1+e^{ika} & 1 \\ 1+e^{-ika} & 0 & 0 \\ 1 & 0 & 0 \end{pmatrix}, \tag{2}$$

where a denotes the lattice spacing. The corresponding bulk spectrum consists of two dispersive bands $E_\pm(k) = \pm t\sqrt{3+2\cos(ak)}$ as well as one completely flat band $E_0(k) = 0$ that is separated from the dispersive bands by an energy gap, see Fig. 1(b). The flat band is macroscopically degenerate and is spanned by a set of N linearly independent states. These can be chosen to have support on only three lattice sites each: $|v_n\rangle = (|n, C\rangle - |n, B\rangle + |n+1, C\rangle)/\sqrt{3}$ for $n \in \{1, ..., N\}$. One of these so-called compact localized states (CLSs) [57] is visualized in Fig. 1(a). While the CLSs are chosen such that they are strictly localized, they are not mutually orthogonal. In order to construct a set of mutually orthogonal basis states for the flat band, the strict localization has to be traded in for exponential localization, e.g., by changing to a basis of maximally localized Wannier states.

As a second example, we introduce the diamond lattice depicted in Fig. 1(c). Again, the unit cell consists of three atoms labeled A, B, and C, and neighboring lattice sites are coupled by a hopping element of strength t. The Hamiltonian then reads

$$H_{\text{dia}} = t\sum_n (c^\dagger_{n,A}c_{n,B} + c^\dagger_{n,A}c_{n,C} + c^\dagger_{n+1,A}c_{n,B} + c^\dagger_{n+1,A}c_{n,C}) + \text{H.c.} \tag{3}$$

In momentum space, this leads to $H_{\text{dia}} = \sum_k \Psi^\dagger_k \mathcal{H}(k)\Psi_k$ with

$$\mathcal{H}(k) = t\begin{pmatrix} 0 & 1+e^{ika} & 1+e^{ika} \\ 1+e^{-ika} & 0 & 0 \\ 1+e^{-ika} & 0 & 0 \end{pmatrix}. \tag{4}$$

Again, the bulk spectrum consists of two dispersive bands $E_\pm(k) = \pm 2\sqrt{2}t\cos(ka/2)$ and a flat band $E_0(k) = 0$, see Fig. 1(d). Importantly, however, there is now no energy gap separating the flat band from the dispersive bands. Rather, the two dispersive bands intersect the flat band in a linear band touching point. Nevertheless, the flat band can again be described in terms of a set of CLSs having support on two lattice sites each, see Fig. 1(c). Explicitly, their wave functions are given by $|v_n\rangle = (|n, C\rangle - |n, B\rangle)/\sqrt{2}$.

RKKY interaction. We now calculate the RKKY interaction between two classical magnetic impurities on the stub and diamond lattice. For this, we consider a system of spinful electrons with both spin species independently described by H_{stub} or H_{dia}, respectively. Additionally, two magnetic impurities are placed in the unit cells n_1 and n_2 at the sublattice positions α and β, respectively. The local exchange coupling to the impurities can then be described as $H^{(1)}_{imp} + H^{(2)}_{imp}$ with

$$H^{(i)}_{imp} = \frac{J_i}{2}\sum_{\sigma,\sigma'} c^\dagger_{n_i,l_i,\sigma}\left[\mathbf{S}_i \cdot \boldsymbol{\sigma}\right]^{\sigma\sigma'} c_{n_i,l_i,\sigma'}, \tag{5}$$

where we have defined $l_1 = \alpha$ and $l_2 = \beta$. Compared to Eqs. (1) and (3), the electronic creation (annihilation) operators $c^\dagger_{n,l,\sigma}$ ($c_{n,l,\sigma}$) now carry an additional spin label $\sigma \in \{\uparrow, \downarrow\}$. Furthermore, $\boldsymbol{\sigma}$ is the vector of Pauli matrices, $\mathbf{S}_i$ are classical impurity spins with $S_i = |\mathbf{S}_i| \gg 1$, and J_i denotes the exchange coupling between the impurity spin and the electron spin density. We assume $\mathbf{S}_i = (0, 0, \pm S_i)$ without loss of generality.

The standard expression for the RKKY interaction in second-order perturbation theory is then

$$J^{\alpha\beta}_{RKKY} = -\frac{J_1 J_2}{2\pi}\int_{-\infty}^{0} dE\, \text{Im}[G^{(0)}_{\alpha\beta}(R, E)G^{(0)}_{\beta\alpha}(-R, E)], \tag{6}$$

where $G^{(0)}_{\alpha\beta}$ is the retarded single-particle Green function of the unperturbed system and $R = r_2 - r_1 = (n_2 - n_1)a > 0$. However, in our case, we would like to avoid the usual perturbative approach as its validity for flat-band systems is not clear *a priori*. Instead, we calculate $J^{\alpha\beta}_{RKKY}$ exactly by numerically computing the exact ground state energies $E^{\alpha\beta}_{FM}$ and $E^{\alpha\beta}_{AFM}$ for the ferromagnetic (FM) and

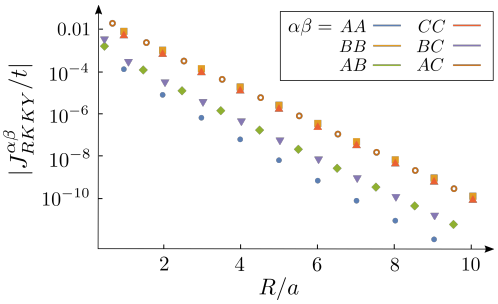

FIG. 2. Absolute value of the RKKY coupling $|J^{\alpha\beta}_{RKKY}|$ in the stub lattice in dependence on the inter-impurity distance R, calculated via ED and displayed in a logarithmic scale. For all sublattice configurations, $|J^{\alpha\beta}_{RKKY}|$ decays exponentially exponentially with R. Here, we set $J_1 = J_2 = 0.2t$.

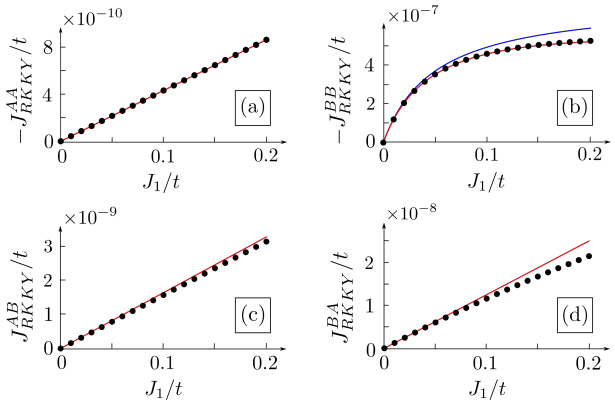

FIG. 3. RKKY coupling $J^{\alpha\beta}_{RKKY}$ in the stub lattice in dependence on the exchange coupling J_1 calculated via ED (dots) and perturbation theory (lines). (a) AA configuration. Here, $J^{AA}_{RKKY} \propto J_1$ as expected from Eq. (6) (red line). (b) BB configuration. Here, J^{BB}_{RKKY} shows an unconventional behavior due to a first-order contribution (blue line) originating from the degenerate flat band. The red line additionally includes the second-order contribution. (c) AB configuration. Here, $J^{AB}_{RKKY} \propto J_1$ with a slope that is well approximated by Eq. (6) (red line). (d) BA configuration. Here, $J^{BA}_{RKKY} \propto J_1$ to lowest order (red line). As J_1 increases, an unconventional third-order term $\propto J_1^2 J_2$ originating from the flat band becomes important. In all panels, we set $J_2/t = 0.05$ and $R/a = 5$.

the antiferromagnetic (AFM) configuration of the impurities, respectively. This gives us

$$J^{\alpha\beta}_{RKKY} = (E^{\alpha\beta}_{FM} - E^{\alpha\beta}_{AFM})/2. \tag{7}$$

The energies $E^{\alpha\beta}_{FM}$ and $E^{\alpha\beta}_{AFM}$ can be computed via exact diagonalization (ED) [35]. Alternatively, we can also calculate the ground state energies in terms of the exact lattice Green functions using the optimized algorithm presented in the SM [76]. This allows us to study significantly larger system sizes while at the same time improving the numerical accuracy of our results.

We start by discussing the stub lattice. First, we look at the dependence of $J^{\alpha\beta}_{RKKY}$ on the inter-impurity distance R. By ED, we find that $J^{\alpha\beta}_{RKKY}$ decays exponentially with R for all sublattice configurations, see Fig. 2. For the AA configuration, this is obvious since the eigenstates spanning the flat band do not have support on the A sublattice. As such, J^{AA}_{RKKY} is exponentially suppressed with the energy gap between the two dispersive bands like for a conventional insulator [77]. For the other sublattice configurations, the flat band participates in mediating the RKKY interaction. However, the flat-band states are spatially localized (e.g., they can be constructed as exponentially localized Wannier states), such that their contribution is exponentially suppressed with R as well. Furthermore, in accordance with the general result for bipartite lattices at half filling [29], we find that the ground state is FM (AFM) if the two impurities are located on the same (on different) sublattices of the bipartition [78].

Next, in order to gain further insight into the nature of the RKKY interaction, we study $J^{\alpha\beta}_{RKKY}$ in dependence on one of the exchange coupling constants—say, J_1—for $J_{1,2}/t \ll 1$. For the AA configuration [Fig. 3(a)] we find that $J^{AA}_{RKKY} \propto J_1$ as expected from Eq. (6). Indeed, since the flat-band states do not have support on the A sublattice, the standard RKKY approximation can be applied without any caveats. For the BB configuration [Fig. 3(b)], however, we find a more complicated dependence that cannot be described by Eq. (6). This is because Eq. (6) does not take into account the large degeneracy of the flat band. Instead, *degenerate* perturbation theory—controlled by the ratio between $J_{1,2}$ and the energy gap that separates the flat from the dispersive band—should be used to accurately capture the effect of the flat band. This gives a non-vanishing first-order contribution to $J^{\alpha\beta}_{RKKY}$ that is responsible for the unusual J_1-dependence shown in Fig. 3(b). To calculate this contribution, we construct a set of flat-band basis states by applying the Gram-Schmidt orthogonalization method to the set of CLSs illustrated in Fig. 1(a). It is straightforward to see that we can always construct $N-2$ basis states that do not have support on the impurity sites, such that the entire first-order contribution is contained in an effective 2×2 Hamiltonian that results from projecting $H^{(1)}_{imp} + H^{(2)}_{imp}$ onto the remaining two basis states. Assuming $J_{1,2} \geq 0$, we then find that the RKKY coupling is, to first order, given by

$$J_{RKKY} = aJ_1 + bJ_2 - \sqrt{a^2 J_1^2 + b^2 J_2^2 + cJ_1 J_2} \tag{8}$$

for real coefficients a, b, c that correspond to overlap integrals of the participating flat-band basis states. We calculate these coefficients numerically and display the result in Fig. 3(b). We see that for small enough J_1, we get a good agreement with the exact result. As J_1 gets larger also the second-order contribution can be taken into account to get a better match. Lastly, we study the AB [BA] configuration, see Fig. 3(c) [Fig. 3(d)]. Here, Eq. (6) gives the correct lowest-order approximation. As

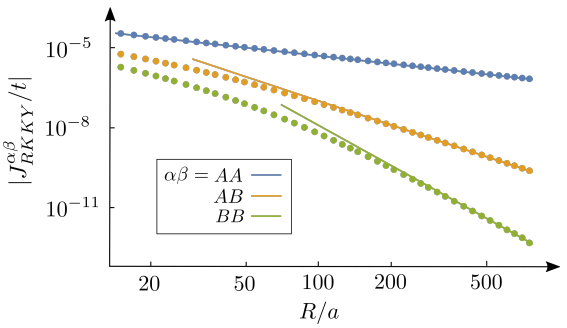

FIG. 4. Absolute value of the RKKY coupling $|J^{\alpha\beta}_{RKKY}|$ in the diamond lattice in dependence on the inter-impurity distance R displayed in a log-log scale. The dots correspond to numerically calculated data using the algorithm described in the SM [76], while the solid lines are the asymptotic analytical expressions given in Eqs. (11)–(13). For the AA configuration, we find the usual $1/R$ decay that is expected in 1D metals. For the other sublattice configurations, the flat band leads to an unusual asymptotic $1/R^3$ ($1/R^5$) decay for the AB (BB) case. Here, we set $J_1 = J_2 = 0.2t$.

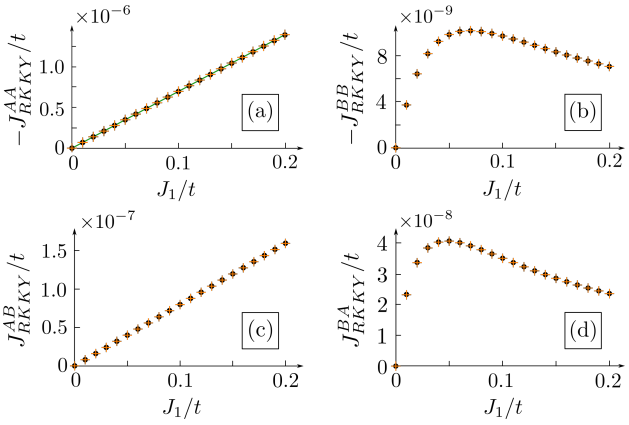

FIG. 5. RKKY coupling $J^{\alpha\beta}_{RKKY}$ in the diamond lattice in dependence on J_1 calculated via ED (black dots) and via Eq. (10) (orange crosses). (a) AA configuration. Here, $J^{AA}_{RKKY} \propto J_1$ as expected from Eq. (6) (green line). (b) BB configuration. Here we find that J^{BB}_{RKKY} increases only for very small J_1/t before it starts to decrease. (c) AB configuration. Here, we again have $J^{AB}_{RKKY} \propto J_1$. (d) BA configuration. Here, J^{BA}_{RKKY} shows an unconventional behavior that is qualitatively similar to panel (b). In all panels, we set $J_2/t = 0.05$ and $R/a = 100$.

J_1 gets larger, an unconventional third-order contribution $\propto J_1 J_2^2$ [$\propto J_1^2 J_2$] originating from the flat band gets important.

Next, we turn to the diamond lattice. Our numerical results for the RKKY interaction in dependence on the inter-impurity distance R are shown in Fig. 4. We display only the AA, BB, AB, and BC configurations since, by symmetry, the CC (AC) configuration is equivalent to the BB (AB) configuration. Again, we find that the ground state is FM (AFM) if the two impurities are located on the same (on different) sublattices of the bipartition. Furthermore, $J^{\alpha\beta}_{RKKY}$ decays as a power law in R with a leading exponent that depends on the sublattice configuration. For the AA configuration, we find that J^{AA}_{RKKY} decays as $1/R$. Again, this is not surprising since the flat-band states do not have support on the A sublattice. As such, we expect to find the same qualitative behavior as in a conventional 1D metal. However, when one (both) impurities are placed on the B or C sublattices, the flat band leads to an unusual $1/R^3$ ($1/R^5$) decay. We will show later that this unusual behavior is non-perturbative in origin.

Next, we can again study the dependence on J_1 for small $J_{1,2}/t$. For the AA configuration [Fig. 5(a)], we again find that $J^{AA}_{RKKY} \propto J_1$ as expected from Eq. (6). For the AB configuration [Fig. 5(c)], we find $J^{AB}_{RKKY} \propto J_1$ as well, but Eq. (6) cannot reasonably approximate the corresponding slope. The BB and BA configurations [Figs. 5(b) and (d)] show an even more peculiar behavior: Here, the RKKY interaction first grows rapidly for very small J_1 but then decreases. This observation makes it highly questionable whether perturbation theory is applicable at all, and the following paragraphs will show that it is indeed not. To see this, we use the T-matrix formalism to obtain an exact expression for the impurity-induced shift to the ground state energy in the FM/AFM configuration. Since spin is conserved, we focus on the two spin sectors individually in the following. In the SM [76], we show that the impurity-induced change in the density of states in a given spin sector and for a given impurity configuration can be written as

$$\Delta\rho(E) = -\frac{1}{\pi}\mathrm{Im}\,\mathrm{tr}\sum_{i,j}\int\frac{dk}{2\pi}[G^{(0)}(k,E)]^2 e^{ik(r_j-r_i)}T_{ij}(E), \tag{9}$$

where $G^{(0)}(k,E)$ is the momentum-space Green function of the unperturbed system and $T_{ij}(E)$ for $i,j \in \{1,2\}$ are the components of the standard two-impurity T-matrix [79]. This can be used to express $J^{\alpha\beta}_{RKKY}$ as

$$J^{\alpha\beta}_{RKKY} = \frac{1}{2}\sum_\sigma \int_{-\infty}^{0} dE\, E\,[\Delta\rho_{FM,\sigma}(E) - \Delta\rho_{AFM,\sigma}(E)]. \tag{10}$$

In Fig. 5, we present our results for $J^{\alpha\beta}_{RKKY}$ obtained from numerically performing the integration over energy in Eq. (10) and find that this reproduces the results from ED very well. Even more interestingly, Eq. (10) can be approximated analytically in the limit of large R and small $J_{1,2}/t$. Following the steps outlined in the SM [76], this leads us to

$$J^{AA}_{RKKY} \approx -\frac{J_1 J_2}{16\sqrt{2}t\pi(R/a)}, \tag{11}$$

$$J^{AB}_{RKKY} \approx \frac{J_1 t}{2\sqrt{2}\pi J_2 (R/a)^3}, \tag{12}$$

$$J^{BB}_{RKKY} \approx -\frac{12\sqrt{2}\,t^3}{\pi J_1 J_2 (R/a)^5}. \tag{13}$$

We plot these approximations in Fig. 4 and find that they nicely approach the numerical curves for large enough R, thereby confirming the power laws we previously read off from our numerical data. Importantly, for sufficiently large R, Eqs. (11)-(13) hold down to arbitrarily small but finite $J_{1,2}$. As such, the results for the AB and BB configuration show a highly non-perturbative behavior. The above relations further confirm our findings from Fig. 5, where we observed qualitatively that the RKKY interaction grows linearly with J_1 if the first impurity is on the A sublattice, while it decreases with J_1 if the impurity is on the B sublattice. However, in this case, the asymptotic $1/J_1$ behavior was not yet clearly visible since the impurity separation was not large enough.

Conclusions. We have studied the RKKY interaction in two 1D flat-band models at half filling. In our first example—the stub lattice—we have found an unconventional first-order contribution to the RKKY interaction due to the degeneracy of the isolated flat band. In our second example—the diamond lattice—the absence of an energy gap between the flat and the dispersive bands leads to a breakdown of perturbation theory altogether, and non-perturbative contributions cause the RKKY interaction to decay more rapidly with the inter-impurity distance than naïvely expected. Our results illustrate that the RKKY interaction in flat-band systems can exhibit unexpected features and has to be treated with care. We expect this to be relevant in particular for Moiré materials such as, e.g., twisted bilayer or trilayer graphene, which can host isolated flat bands [58–63] or intersecting flat and Dirac-like bands [80–85], respectively.

Of course, it is now interesting to ask how our results are modified by, e.g., electron-electron interactions or disorder. We leave these questions to future work. Furthermore, we have focused on the case of a perfectly flat band at half-filling, where we expect flat-band effects to be the most pronounced. Nevertheless, it would also be interesting to study more general fillings and small deviations from perfect flatness. In general, as long as the exchange coupling constants are larger than any additional energy scale resulting, e.g., from a small but finite bandwidth, we expect the unconventional effects reported here to persist.

Acknowledgments. We thank Henry F. Legg for helpful discussions. This work was supported by the Deutsche Forschungsgemeinschaft via RTG 1995, the Swiss National Science Foundation (SNSF) and NCCR QSIT and by the Deutsche Forschungsgemeinschaft (DFG, German Research Foundation) under Germany's Excellence Strategy - Cluster of Excellence Matter and Light for Quantum Computing (ML4Q) EXC 2004/1 - 390534769. We acknowledge support from the Max Planck-New York City Center for Non-Equilibrium Quantum Phenomena. This project received funding from the European Union's Horizon 2020 research and innovation program (ERC Starting Grant, grant agreement No 757725). Simulations were performed with computing resources granted by RWTH Aachen University under projects rwth0752 and rwth0841.

Note added: During the finalization of this manuscript, we became aware of a related recent study [94].

[1] M. A. Rudermann and C. Kittel, Phys. Rev. **96**, 99 (1954).
[2] T. Kasuya, Prog. Theor. Phys. **16**, 45 (1956).
[3] K. Yosida, Phys. Rev. **106**, 893 (1957).
[4] P. Bruno and C. Chappert, Phys. Rev. Lett. **67**, 1602 (1991).
[5] P. Bruno and C. Chappert, Phys. Rev. B **46**, 261 (1992).
[6] N. J. Craig, J. M. Taylor, E. A. Lester, C. M. Marcus, M. P. Hanson, and A. C. Gossard, Science **304**, 565 (2004).
[7] L. I. Glazman and R. C. Ashoori, Science **304**, 524 (2004).
[8] G. Usaj, P. Lustemberg, and C. A. Balseiro, Phys. Rev. Lett. **94**, 036803 (2005).
[9] P. Simon, R. López, and Y. Oreg, Phys. Rev. Lett. **94**, 086602 (2005).
[10] G. Yang, C.-H. Hsu, P. Stano, J. Klinovaja, and D. Loss, Phys. Rev. B **93**, 075301 (2016).
[11] A. A. Khajetoorians, J. Wiebe, B. Chilian, and R. Wiesendanger, Science **332**, 1062 (2011).
[12] M. Steinbrecher, R. Rausch, K. T. That, J. Hermenau, A. A. Khajetoorians, M. Potthoff, R. Wiesendanger, and J. Wiebe, Nat. Comm. **9**, 2853 (2018).
[13] F. Pientka, L. I. Glazman, and F. von Oppen, Phys. Rev. B **88**, 155420 (2013).
[14] B. Braunecker and P. Simon, Phys. Rev. Lett. **111**, 147202 (2013).
[15] J. Klinovaja, P. Stano, A. Yazdani, and D. Loss, Phys. Rev. Lett. **111**, 186805 (2013).
[16] M. M. Vazifeh and M. Franz, Phys. Rev. Lett. **111**, 206802 (2013).
[17] F. Pientka, L. I. Glazman, and F. von Oppen, Phys. Rev. B **89**, 180505(R) (2014).
[18] Y. Kim, M. Cheng, B. Bauer, R. M. Lutchyn, and S. Das Sarma, Phys. Rev. B **90**, 060401(R) (2014).
[19] B. Braunecker and P. Simon, Phys. Rev. B **92**, 241410(R) (2015).
[20] C.-H. Hsu, P. Stano, J. Klinovaja, and D. Loss, Phys. Rev. B **92**, 235435 (2015).
[21] M. Schecter, K. Flensberg, M. H. Christensen, B. M. Andersen, and J. Paaske, Phys. Rev. B **93**, 140503(R) (2016).
[22] R. Pawlak, M. Kisiel, J. Klinovaja, T. Meier, S. Kawai, T. Glatzel, D. Loss, and E. Meyer, npj Quantum Inf. **2**, 16035 (2016).
[23] R. Pawlak, S. Hoffman, J. Klinovaja, D. Loss, and E. Meyer, Progress in Particle and Nuclear Physics **107**, 1 (2019).
[24] A. Y. Zyuzin and B. Z. Spivak, JETP Lett. **43**, 234 (1986).
[25] D. Poilblanc, D. J. Scalapino, and W. Hanke, Phys. Rev. Lett. **72**, 884 (1994).
[26] A. V. Balatsky, M. I. Salkola, and A. Rosengren, Phys.

Rev. B **51**, 15547 (1995).
[27] V. M. Galitski and A. I. Larkin, Phys. Rev. B **66**, 064526 (2002).
[28] H. Imamura, P. Bruno, and Y. Utsumi, Phys. Rev. B **69**, 121303(R) (2004).
[29] S. Saremi, Phys. Rev. B **76**, 184430 (2007).
[30] E. H. Hwang and S. Das Sarma, Phys. Rev. Lett. **101**, 156802 (2008).
[31] B. Braunecker, P. Simon, and D. Loss, Phys. Rev. Lett. **102**, 116403 (2009).
[32] J. Gao, W. Chen, X. C. Xie, and F.-c. Zhang, Phys. Rev. B **80**, 241302(R) (2009).
[33] Q. Liu, C.-X. Liu, C. Xu, X.-L. Qi, and S.-C. Zhang, Phys. Rev. Lett. **102**, 156603 (2009).
[34] I. Garate and M. Franz, Phys. Rev. B **81**, 172408 (2010).
[35] A. M. Black-Schaffer, Phys. Rev. B **81**, 205416 (2010).
[36] A. M. Black-Schaffer, Phys. Rev. B **82**, 073409 (2010).
[37] B. Braunecker, G. I. Japaridze, J. Klinovaja, and D. Loss, Phys. Rev. B **82**, 045127 (2010).
[38] S. Chesi and D. Loss, Phys. Rev. B **82**, 165303 (2010).
[39] J.-J. Zhu, D.-X. Yao, S.-C. Zhang, and K. Chang, Phys. Rev. Lett. **106**, 097201 (2011).
[40] D. A. Abanin and D. A. Pesin, Phys. Rev. Lett. **106**, 136802 (2011).
[41] M. Sherafati and S. Satpathy, Phys. Rev. B **83**, 165425 (2011).
[42] E. Kogan, Phys. Rev. B **84**, 115119 (2011).
[43] J. Klinovaja and D. Loss, Phys. Rev. B **87**, 045422 (2013).
[44] S. R. Power and M. S. Ferreira, Crystals **3**, 49 (2013).
[45] N. Y. Yao, L. I. Glazman, E. A. Demler, M. D. Lukin, and J. D. Sau, Phys. Rev. Lett. **113**, 087202 (2014).
[46] A. A. Zyuzin and D. Loss, Phys. Rev. B **90**, 125443 (2014).
[47] D. K. Efimkin and V. Galitski, Phys. Rev. B **89**, 115431 (2014).
[48] M. Schecter, M. S. Rudner, and K. Flensberg, Phys. Rev. Lett. **114**, 247205 (2015).
[49] A. M. Tsvelik and O. M. Yevtushenko, Phys. Rev. Lett. **119**, 247203 (2017).
[50] V. D. Kurilovich, P. D. Kurilovich, and I. S. Burmistrov, Phys. Rev. B **95**, 115430 (2017).
[51] C.-H. Hsu, P. Stano, J. Klinovaja, and D. Loss, Phys. Rev. B **96**, 081405(R) (2017).
[52] C.-H. Hsu, P. Stano, J. Klinovaja, and D. Loss, Phys. Rev. B **97**, 125432 (2018).
[53] H. F. Legg and B. Braunecker, Sci. Rep. **9**, 17697 (2019).
[54] O. Deb, S. Hoffman, D. Loss, and J. Klinovaja, Phys. Rev. B **103**, 165403 (2021).
[55] K. Laubscher, D. Miserev, V. Kaladzhyan, D. Loss, and J. Klinovaja, arXiv:2203.08137.
[56] Z. Liu, F. Liu, and Y.-S. Wu, Chinese Phys. B **23**, 077308 (2014).
[57] D. Leykam, A. Andreanov, and S. Flach, Adv. Phys. **3**, 1473052 (2018).
[58] R. Bistritzer and A. H. MacDonald, Proc. Natl. Acad. Sci. USA **108**, 12233 (2011).
[59] Y. Cao, V. Fatemi, A. Demir, S. Fang, S. L. Tomarken, J. Y. Luo, J. D. Sanchez-Yamagishi, K. Watanabe, T. Taniguchi, E. Kaxiras, R. C. Ashoori, and P. Jarillo-Herrero, Nature **556**, 80 (2018).
[60] Y. Cao, V. Fatemi, S. Fang, K. Watanabe, T. Taniguchi, E. Kaxiras, P. Jarillo-Herrero, Nature **556**, 43 (2018).
[61] A. H. MacDonald, Physics **12**, 12 (2019).
[62] E. Y. Andrei and A. H. MacDonald, Nat. Mater. **19**, 1265 (2020).
[63] L. Balents, C. R. Dean, D. K. Efetov, and A. F. Young, Nat. Phys. **16**, 725 (2020).
[64] E. H. Lieb, Phys. Rev. Lett. **62**, 1201 (1989).
[65] B. Sutherland, Phys. Rev. B **34**, 5208 (1986).
[66] R. Shen, L. B. Shao, B. Wang, and D. Y. Xing, Phys. Rev. B **81**, 041410 (2010).
[67] V. Apaja, M. Hyrkäs, and M. Manninen, Phys. Rev. A **82**, 041402 (2010).
[68] T. Zhang and G.-B. Jo, Sci. Rep. **5**, 16044 (2015).
[69] M. R. Slot, T. S. Gardenier, P. H. Jacobse, G. C. P. van Miert, S. N. Kempkes, S. J. M. Zevenhuizen, C. Morais Smith, D. Vanmaekelbergh, and I. Swart, Nature Phys. **13**, 672 (2017).
[70] S. Xia, A. Ramachandran, S. Xia, D. Li, X. Liu, L. Tang, Y. Hu, D. Song, J. Xu, D. Leykam, S. Flach, and Z. Chen, Phys. Rev. Lett. **121**, 263902 (2018).
[71] M. N. Huda, S. Kezilebieke, and P. Liljeroth, Phys. Rev. Research **2**, 043426 (2020).
[72] J. E. Bunder and H.-H. Lin, Phys. Rev. B **80**, 153414 (2009).
[73] J. Cao, H. A. Fertig, and S. Zhang, Phys. Rev. B **99**, 205430 (2019).
[74] D. O. Oriekhov and V. P. Gusynin, Phys. Rev. B **101**, 235162 (2020).
[75] G. Bouzerar, arXiv:2106.10117.
[76] In the Supplemental Material, we give the Green functions for the diamond lattice, derive Eq. (9), and provide details on how to approximate Eq. (10) for large R and small $J_{1,2}$. Furthermore, we present an optimized algorithm that computes the RKKY coupling numerically using lattice Green functions.
[77] N. Bloembergen and T. J. Rowland, Phys. Rev. **97**, 1679 (1955).
[78] We note, however, that the results in Ref. [29] were obtained from a perturbative approach rather than an exact one.
[79] E. N. Economou, *Green's Functions in Quantum Physics*, third edition (Springer, Berlin, 2006).
[80] E. Khalaf, A. J. Kruchkov, G. Tarnopolsky, and A. Vishwanath, Phys. Rev. B **100**, 085109 (2019).
[81] S. Carr, C. Li, Z. Zhu, E. Kaxiras, S. Sachdev, and A. Kruchkov, Nano Lett. **20**, 3030 (2020).
[82] C. Lei, L. Linhart, W. Qin, F. Libisch, and A. H. MacDonald, Phys. Rev. B **104**, 035139 (2021).
[83] H. Kim, Y. Choi, C. Lewandowski, A. Thomson, Y. Zhang, R. Polski, K. Watanabe, T. Taniguchi, J. Alicea, S. Nadj-Perge, arXiv:2109.12127.
[84] C. Shen, P. J. Ledwith, K. Watanabe, T. Taniguchi, E. Khalaf, A. Vishwanath, D. K. Efetov, arXiv:2204.07244.
[85] Y. Li, S. Zhang, F. Chen, L. Wei, Z. Zhang, H. Xiao, H. Gao, M. Chen, S. Liang, D. Pei, L. Xu, K. Watanabe, T. Taniguchi, L. Yang, F. Miao, J. Liu, B. Cheng, M. Wang, Y. Chen, Z. Liu, arXiv:2209.02199.
[86] N. Müller, D. M. Kennes, J. Klinovaja, D. Loss, and H. Schoeller, Phys. Rev. B **101**, 155417 (2020).
[87] S. Andergassen, T. Enss, V. Meden, W. Metzner, U. Schollwöck, and K. Schönhammer, Phys. Rev. B **70**, 075102 (2004).
[88] F. Guinea, C. Tejedor, F. Flores, and E. Louis, Phys. Rev. B **28**, 4397 (1983).
[89] M. P. Lopez Sancho, J. M. Lopez Sancho, and J. Rubio, J. Phys. F: Met. Phys. **15**, 851 (1985).

[90] C. H. Lewenkopf and E. R. Mucciolo, Journal of Computational Electronics **12**, 203 (2013).
[91] M. M. Odashima, B. G. Prado, and E. Vernek, Rev. Bras. Ens. Fis. **39**, e1303 (2017).
[92] K. S. Dy, Shi-Yu Wu, and T. Spratlin, Phys. Rev. B **20**, 4237 (1979).
[93] G. Meurant, SIAM J. Matrix Anal. Appl. **13**, 707 (1992).
[94] G. Bouzerar, arXiv:2210.08896.

Supplemental Material: RKKY interaction in one-dimensional flat band lattices

Katharina Laubscher,[1] Clara S. Weber,[2,3] Maximilian Hünenberger,[1] Herbert Schoeller,[2] Dante M. Kennes,[2,4] Daniel Loss,[1] and Jelena Klinovaja[1]

[1]*Department of Physics, University of Basel, Klingelbergstrasse 82, CH-4056 Basel, Switzerland*
[2]*Institut für Theorie der Statistischen Physik, RWTH Aachen, 52056 Aachen, Germany and JARA - Fundamentals of Future Information Technology*
[3]*Department of Physics and Astronomy, University of Pennsylvania, Philadelphia, Pennsylvania 19104, USA*
[4]*Max Planck Institute for the Structure and Dynamics of Matter, Center for Free Electron Laser Science, 22761 Hamburg, Germany*

In this Supplemental Material, we give the real-space Matsubara Green functions for the diamond lattice, derive Eq. (9) in the main text, and provide details on how to approximate Eq. (10) in the main text for large R and small $J_{1,2}$. Furthermore, we present an optimized algorithm that computes the RKKY coupling numerically using the full lattice Green functions of the perturbed system.

To simplify the notation, we set $a = t = 1$ throughout this Supplemental Material.

S1. MATSUBARA GREEN FUNCTIONS FOR THE DIAMOND LATTICE

In this Appendix, we list the Matsubara Green functions for the diamond lattice. For $r \geq 0$ and $\omega \neq 0$, we find:

$$G^{(0)}_{AA}(r, i\omega) = \frac{-i\left[-1 + \frac{\omega}{4}(-\omega + \gamma)\right]^r}{\gamma}, \tag{S1}$$

$$G^{(0)}_{AB}(r, i\omega) = \frac{4^{-1-r}(\omega - \gamma)\left[-4 + \omega(-\omega + \gamma)\right]^r}{\gamma}, \tag{S2}$$

$$G^{(0)}_{BB}(r, i\omega) = -i\left(\frac{\left[-1 + \frac{\omega}{4}(-\omega + \gamma)\right]^r}{2\gamma} + \frac{\delta_{r,0}}{2\omega}\right), \tag{S3}$$

$$G^{(0)}_{BC}(r, i\omega) = -i\left(\frac{\left[-1 + \frac{\omega}{4}(-\omega + \gamma)\right]^r}{2\gamma} - \frac{\delta_{r,0}}{2\omega}\right), \tag{S4}$$

$$G^{(0)}_{BA}(r, i\omega) = \frac{4^{-1-r}(\omega + \gamma)\left[-4 + \omega(-\omega + \gamma)\right]^r}{\gamma} - \frac{\delta_{r,0}}{2}, \tag{S5}$$

where we have defined $\gamma = \mathrm{sgn}(\omega)\sqrt{8 + \omega^2}$. The other components can be obtained from the above as $G^{(0)}_{AC} = G^{(0)}_{AB}$, $G^{(0)}_{CA} = G^{(0)}_{BA}$, $G^{(0)}_{CB} = G^{(0)}_{BC}$, and $G^{(0)}_{CC} = G^{(0)}_{BB}$, where we omitted the frequency argument for brevity. The Green functions for $r < 0$ can be found from the relation $G^{(0)}_{\alpha\beta}(r, i\omega) = [G^{(0)}_{\beta\alpha}(-r, -i\omega)]^*$.

S2. IMPURITY-INDUCED CHANGE IN THE DENSITY OF STATES

In this Appendix, we derive Eq. (9) in the main text. Using the two-impurity T-matrix, the full Green function of the perturbed system can be expressed as

$$G(r, r', E) = G^{(0)}(r - r', E) + \sum_{i,j} G^{(0)}(r - r_i, E) T_{ij}(E) G^{(0)}(r_j - r', E), \tag{S6}$$

where $i, j \in \{1, 2\}$. The four components of the two-impurity T-matrix are given by [1]:

$$T_{11}(E) = \left[\mathbb{1} - V_1 G^{(0)}(0, E) - V_1 G^{(0)}(-R, E) T^{(0)}_2(E) G^{(0)}(R, E)\right]^{-1} V_1, \tag{S7}$$

$$T_{12}(E) = T^{(0)}_1(E) G^{(0)}(-R, E) T_{22}(E), \tag{S8}$$

$$T_{21}(E) = T^{(0)}_2(E) G^{(0)}(R, E) T_{11}(E), \tag{S9}$$

$$T_{22}(E) = \left[\mathbb{1} - V_2 G^{(0)}(0, E) - V_2 G^{(0)}(R, E) T^{(0)}_1(E) G^{(0)}(-R, E)\right]^{-1} V_2, \tag{S10}$$

where we have defined $V_1 = \pm\frac{J_1}{2}|\alpha\rangle\langle\alpha|$ and $V_2 = \pm\frac{J_2}{2}|\beta\rangle\langle\beta|$, where each of the four different sign combinations corresponds to a choice of spin sector and relative orientation (FM/AFM) of the two impurities. Moreover, we have defined the single-impurity T-matrices as

$$T_i^{(0)} = \Big[\mathbb{1} - V_i G^{(0)}(0,E)\Big]^{-1} V_i. \tag{S11}$$

The unperturbed Green functions for the diamond lattice that enter the above expressions are given in Sec. S1.

The exact Green function can then be used to obtain the impurity-induced change in the local density of states (DoS) of the system:

$$\Delta\rho(r,E) = -\frac{1}{\pi}\mathrm{Im\,tr}[G(r,r,E) - G^{(0)}(0,E)] \tag{S12}$$

$$= -\frac{1}{\pi}\mathrm{Im\,tr}\Big[\sum_{ij} G^{(0)}(r-r_i,E)T_{ij}(E)G^{(0)}(r_j-r,E)\Big]. \tag{S13}$$

From this, we obtain the total change of the DoS due to a given impurity configuration as

$$\begin{aligned}\Delta\rho(E) &= \int dr\,\Delta\rho(r,E)\\ &= -\frac{1}{\pi}\mathrm{Im\,tr}\sum_{ij}\int dr\,G^{(0)}(r-r_i,E)T_{ij}(E)G^{(0)}(r_j-r,E)\\ &= -\frac{1}{\pi}\mathrm{Im\,tr}\sum_{ij}\int\frac{dk}{2\pi}\int\frac{dk'}{2\pi}\int dr\,e^{i(k'-k)r}G^{(0)}(k,E)G^{(0)}(k',E)e^{ikr_j}e^{-ik'r_i}T_{ij}(E)\\ &= -\frac{1}{\pi}\mathrm{Im\,tr}\sum_{ij}\int\frac{dk}{2\pi}[G^{(0)}(k,E)]^2e^{ik(r_j-r_i)}T_{ij}(E).\end{aligned} \tag{S14}$$

This is Eq. (9) of the main text.

S3. ASYMPTOTIC EXPRESSIONS FOR THE RKKY COUPLING

In this Appendix, we extract the asymptotic behavior of Eq. (10) in the main text in the limit of large R. For convenience, we write $J_{RKKY}^{\alpha\beta} = \sum_{i,j} J_{RKKY}^{\alpha\beta,ij}$ with

$$J_{RKKY}^{\alpha\beta,ij} = \frac{1}{2}\sum_\sigma\int_{-\infty}^0 dE\,E\,[\Delta\rho_{FM,\sigma}^{ij}(E) - \Delta\rho_{AFM,\sigma}^{ij}(E)], \tag{S15}$$

$$\Delta\rho^{ij}(E) = -\frac{1}{\pi}\mathrm{Im\,tr}\int\frac{dk}{2\pi}[G^{(0)}(k,E)]^2e^{ik(r_j-r_i)}T_{ij}(E). \tag{S16}$$

We start by discussing the AA configuration. In this case, the flat band is not affected by the impurities and we can safely expand the full T-matrix in orders of $J_{1,2}$. Since the unperturbed system is time-reversal symmetric, first-order contributions to the RKKY coupling cancel when the two spin sectors are added up. As such, to lowest order, the RKKY coupling is given by second-order terms $\propto J_1J_2$. These terms are contained within the off-diagonal contributions to the RKKY coupling:

$$J_{RKKY}^{AA,12} = J_{RKKY}^{AA,21} = -\frac{J_1J_2}{\pi}\int_0^\infty d\omega\,(-i\omega)\,G_{AA}^{(0)}(R,i\omega)P_{AA}^{(0)}(-R,i\omega), \tag{S17}$$

where we have introduced the short-hand notation $P^{(0)}(r,i\omega) = \int\frac{dk}{2\pi}[G^{(0)}(k,i\omega)]^2e^{ikr}$ and where we have already used that $G_{AA}^{(0)}$ ($P_{AA}^{(0)}$) is purely imaginary (real). Note that we find it convenient to evaluate the above integral in the Matsubara representation. Plugging in the Green functions given in Sec. S1, we find that Eq. (S17) gives us

$$J_{RKKY}^{AA} = -\frac{J_1J_2}{\pi}\int_0^\infty d\omega\,\omega\left[\frac{16^{-R}(4+\omega^2-\omega\gamma)^{2R}(\omega+2\gamma R)}{\gamma^4}\right] \tag{S18}$$

with $\gamma = \sqrt{8+\omega^2}$. The integral converges on a scale $\propto 1/R$, which is why we can change the integration variable to $\omega' = \omega R$ and then cut the upper integration limit at some finite constant C that does not depend on R. This allows us to expand the integrand for small ω'/R in order to obtain the asymptotic behavior at large R. In particular, we can approximate

$$16^{-R}\left[4+\left(\frac{\omega'}{R}\right)^2-\frac{\omega'}{R}\sqrt{8+\left(\frac{\omega'}{R}\right)^2}\right]^{2R} \approx 16^{-R}\left(4-\frac{\sqrt{8}\omega'}{R}\right)^{2R} = \left(1-\frac{\omega'}{\sqrt{2}R}\right)^{2R} \approx e^{-\sqrt{2}\omega'}. \tag{S19}$$

Keeping only the leading contributions also in the rest of the integral, we obtain

$$J^{AA}_{RKKY} \approx -\frac{J_1J_2}{8\sqrt{2}\pi R}\int_0^\infty d\omega'\,\omega' e^{-\sqrt{2}\omega'} = -\frac{J_1J_2}{16\sqrt{2}\pi R}. \tag{S20}$$

After reinstating a and t, this leads us to Eq. (11) in the main text.

In a similar fashion, we can also obtain an asymptotic expression for the AB configuration. Since the second impurity is now sitting on the B sublattice, this impurity will also affect the flat band. In this case, the vanishing band width of the flat band makes it questionable whether we can expand our expression for the RKKY coupling in orders of J_2. We therefore keep the full T-matrix for the second impurity while still expanding in orders of J_1. To lowest order in J_1, we then find two different non-vanishing contributions to the RKKY coupling:

$$J^{AB,12}_{RKKY} = J^{AB,21}_{RKKY} = -\frac{4J_1J_2}{\pi}\int_0^\infty d\omega\,(-i\omega)\,\frac{G^{(0)}_{BA}(R,i\omega)P^{(0)}_{AB}(-R,i\omega)}{4-J_2^2[G^{(0)}_{BB}(0,i\omega)]^2}, \tag{S21}$$

$$J^{AB,22}_{RKKY} = -\frac{4J_1J_2^3}{\pi}\int_0^\infty d\omega\,(-i\omega)\,\frac{G^{(0)}_{BA}(R,i\omega)G^{(0)}_{AB}(-R,i\omega)G^{(0)}_{BB}(0,i\omega)P^{(0)}_{BB}(0,i\omega)}{\left(4-J_2^2[G^{(0)}_{BB}(0,i\omega)]^2\right)^2}. \tag{S22}$$

Plugging in the Green functions, we get

$$J^{AB,12}_{RKKY} = -\frac{8J_1J_2}{\pi}\int_0^\infty d\omega\,\omega\left[\frac{16^{-R}\omega^2(\omega-\gamma)(4+\omega^2-\omega\gamma)^{2R-2}[4+(\omega^2-\omega\gamma)(1-R)-8R]}{\gamma^2[8\omega^2\gamma^2+(4+\omega^2)J_2^2+\omega\gamma J_2^2]}\right], \tag{S23}$$

$$J^{AB,22}_{RKKY} = -\frac{4J_1J_2^3}{\pi}\int_0^\infty d\omega\,\omega\left[\frac{16^{-R}\omega(4+\omega^2-\omega\gamma)^{2R}[-8\gamma+\omega(8+\omega^2-2\omega\gamma)]}{\gamma^5[\omega^2\gamma^2(4+\omega^2-\omega\gamma)+2J_2^2]^2}\right]. \tag{S24}$$

These integrals can be approximated following the same steps as above, and, in particular, using again Eq. (S19). We obtain

$$J^{AB}_{RKKY} = 2J^{AB,12}_{RKKY} + J^{AB,22}_{RKKY} \approx \frac{J_1}{\pi J_2R^3}\int_0^\infty d\omega'\,\left(\frac{\omega'^3}{\sqrt{2}}-\omega'^2\right)e^{-\sqrt{2}\omega'} = \frac{J_1}{2\sqrt{2}\pi J_2R^3}, \tag{S25}$$

which leads us to Eq. (12) in the main text. Finally, for the BB configuration, we now keep the full T-matrices for both impurities. We now get three different non-vanishing contributions to the RKKY coupling:

$$J^{AB,12}_{RKKY} = J^{AB,21}_{RKKY}$$
$$= -\frac{8J_1J_2}{\pi}\int_0^\infty d\omega\,(-i\omega)\frac{G^{(0)}_{BB}(R,i\omega)P^{(0)}_{BB}(-R,i\omega)\{16-4G^{(0)}_{BB}(0,i\omega)^2(J_1^2+J_2^2)+[G^{(0)}_{BB}(0,i\omega)^4-G^{(0)}_{BB}(R,i\omega)^4]J_1^2J_2^2\}}{F_1(R,i\omega)F_2(R,i\omega)}, \tag{S26}$$

$$J^{AB,11}_{RKKY} = \frac{16J_1^3J_2}{\pi}\int_0^\infty d\omega\,(i\omega)\frac{G^{(0)}_{BB}(0,i\omega)P^{(0)}_{BB}(0,i\omega)G^{(0)}_{BB}(R,i\omega)^2\{4-[G^{(0)}_{BB}(0,i\omega)^2-G^{(0)}_{BB}(R,i\omega)^2]J_2^2\}}{F_1(R,i\omega)F_2(R,i\omega)}, \tag{S27}$$

$$J^{AB,22}_{RKKY} = \frac{16J_1J_2^3}{\pi}\int_0^\infty d\omega\,(i\omega)\frac{G^{(0)}_{BB}(0,i\omega)P^{(0)}_{BB}(0,i\omega)G^{(0)}_{BB}(R,i\omega)^2\{4-[G^{(0)}_{BB}(0,i\omega)^2-G^{(0)}_{BB}(R,i\omega)^2]J_1^2\}}{F_1(R,i\omega)F_2(R,i\omega)}, \tag{S28}$$

with $F_{1,2}(R,i\omega) = 16-4G^{(0)}_{BB}(0,i\omega)^2(J_1^2+J_2^2)\pm 8G^{(0)}_{BB}(R,i\omega)^2J_1J_2-[G^{(0)}_{BB}(R,i\omega)^2-G^{(0)}_{BB}(0,i\omega)^2]^2J_1^2J_2^2$ and where we have used that $G^{(0)}_{BB}(R,i\omega) = [G^{(0)}_{BB}(R,-i\omega)]^* = G^{(0)}_{BB}(-R,i\omega)$. After plugging in the Green functions, the full expressions become too involved to be displayed here. Nevertheless, the integrals can be approximated in the same way as before, which leads us to Eq. (13) in the main text:

$$J^{BB}_{RKKY} = 2J^{AB,12}_{RKKY} + J^{AB,11}_{RKKY} + J^{AB,22}_{RKKY} \approx \frac{1}{J_1J_2\pi R^5}\int_0^\infty d\omega'\,\left(-4\sqrt{2}\omega'^5+16\omega'^4\right)e^{-\sqrt{2}\omega'} = -\frac{12\sqrt{2}}{J_1J_2\pi R^5}. \tag{S29}$$

S4. EXACT RESULTS USING GREEN FUNCTIONS

In this Appendix, we present an efficient algorithm that computes the RKKY coupling numerically using the exact lattice Green functions of the full system. For this, we start by noting that the Hamiltonians studied in the main text have a block-tridiagonal structure. The calculation of Green functions for such Hamiltonians, or in general the calculation of inverse matrices of this kind, has been vastly optimized using several methods [2–8]. In this work, we use an algorithm that can efficiently invert block-tridiagonal matrices as described in Ref. [2]. This algorithm is especially efficient if only a few diagonals, rows, or columns of the matrix are needed since it scales linearly with the system size in these cases. In contrast to Ref. [2] we do not study translationally invariant systems due to the presence of impurities. Therefore, we modify the algorithm of Ref. [2] by adding the needed position dependency as shown in Ref. [9] for tridiagonal matrices. For convenience we recapitulate the algorithm here and present its modified version.

Since the Hamiltonian is Hermitian, the matrix that needs to be inverted has the following structure:

$$A = \begin{pmatrix} a_1 & b_1 & & & & \\ b_1^\dagger & a_2 & b_2 & & & \\ & b_2^\dagger & a_3 & b_3 & & \\ & & b_3^\dagger & a_4 & \ddots & \\ & & & \ddots & \ddots & b_{N-1} \\ & & & & b_{N-1}^\dagger & a_N \end{pmatrix}. \tag{S30}$$

Here, the a_n and b_n are the blocks that the matrix consists of and N is the number of diagonal blocks. Using a UDL-decomposition this matrix can be decomposed into $A = UDL$ with matrices of the form

$$U = \begin{pmatrix} 1 & U_1 & & & \\ & 1 & U_2 & & \\ & & \ddots & \ddots & \\ & & & \ddots & U_{N-1} \\ & & & & 1 \end{pmatrix}, \qquad L = \begin{pmatrix} 1 & & & & \\ L_1 & 1 & & & \\ & L_2 & \ddots & & \\ & & \ddots & \ddots & \\ & & & L_{N-1} & 1 \end{pmatrix}, \tag{S31}$$

and a block-diagonal matrix D with blocks D_n for $n \in \{1, \ldots, N\}$. The matrix elements can be calculated using the recursion relations

$$D_L = a_L, \tag{S32}$$
$$U_n = b_n D_{n+1}^{-1}, \tag{S33}$$
$$L_n = D_{n+1}^{-1} b_n^\dagger, \tag{S34}$$
$$\begin{aligned} D_n &= a_n - U_n b_n^\dagger \\ &= a_n - b_n D_{n+1}^{-1} b_n^\dagger \,. \end{aligned} \tag{S35}$$

The inverse of the matrix A can then be decomposed as well and we find $B = A^{-1} = L^{-1} D^{-1} U^{-1}$ with

$$D^{-1} = \begin{pmatrix} D_1^{-1} & & & \\ & D_2^{-1} & & \\ & & \ddots & \\ & & & D_N^{-1} \end{pmatrix}, \qquad U^{-1} = \begin{pmatrix} 1 & -U_1 & U_1U_2 & \cdots & (-1)^{N-1} U_1 \cdots U_{N-1} \\ & 1 & -U_2 & \ddots & \vdots \\ & & \ddots & \ddots & U_{N-2}U_{N-1} \\ & & & \ddots & -U_{N-1} \\ & & & & 1 \end{pmatrix},$$

$$L^{-1} = \begin{pmatrix} 1 & & & & \\ -L_1 & & \ddots & & \\ L_2 L_1 & & \ddots & \ddots & \\ \vdots & & \ddots & -L_{N-2} & 1 \\ (-1)^{N-1} L_{N-1} \cdots L_1 & \cdots & L_{N-1}L_{N-2} & -L_{N-1} & 1 \end{pmatrix}. \tag{S36}$$

The diagonal elements of B can be calculated recursively by exploiting the relations

$$B_{1,1} = D_1^{-1}, \tag{S37}$$

$$\begin{aligned} B_{n+1,n+1} &= D_{n+1}^{-1} + L_n B_{n,n} U_n \\ &= D_{n+1}^{-1} + D_{n+1}^{-1} b_n^\dagger B_{n,n} b_n D_{n+1}^{-1} \,. \end{aligned} \tag{S38}$$

The off-diagonal matrix elements can then be computed as well. With $m \geq n$, we find the recursive formulas

$$B_{n,m+1} = -B_{n,m} U_m, \tag{S39}$$

$$B_{m+1,n} = -L_m B_{m,n}, \tag{S40}$$

such that we are able to calculate all matrix elements. We want to stress that the $B_{i,j}$ are blocks of the inverse matrix B concerning the different unit cells with elements $B_{m,n}^{\alpha,\beta}$ that can be identified with the Green function $G_{\alpha,\beta}(m,n)$.

With these recursion relations we are able to calculate the energy difference, and therefore also the RKKY coupling, by rewriting it as

$$\Delta E = \langle H^{FM} \rangle - \langle H^{AFM} \rangle \tag{S41}$$

$$= \sum_{n,m,\alpha,\beta} H^{FM}_{n\alpha,m\beta} \left\langle c^\dagger_{n,\alpha} c_{m,\beta} \right\rangle_{FM} - \sum_{n,m,\alpha,\beta} H^{AFM}_{n\alpha,m\beta} \left\langle c^\dagger_{n,\alpha} c_{m,\beta} \right\rangle_{AFM} \tag{S42}$$

$$= \frac{1}{2\pi} \int d\omega e^{i\omega 0^+} \left[\left(\sum_{n,m} H^{FM}_{n\alpha,m\beta} G^{FM}_{\beta\alpha}(m,n;i\omega) \right) - \left(\sum_{n,m} H^{AFM}_{n\alpha,m\beta} G^{AFM}_{\beta\alpha}(m,n;i\omega) \right) \right] \tag{S43}$$

Thereby we used that the needed expectation values are given by

$$\langle c^\dagger_{n,\alpha} c_{m,\beta} \rangle = \frac{1}{i} G^<_{\beta\alpha}(m,n;t=0,t'=0) \tag{S44}$$

$$= \frac{1}{2\pi} \int d\omega \, G^<_{\beta\alpha}(m,n;\omega) \tag{S45}$$

$$= -\int d\omega \, n_F(\omega) \left(\frac{1}{\omega - H + i\eta} - \frac{1}{\omega - H - i\eta} \right)_{m\beta,n\alpha} \tag{S46}$$

$$= \lim_{T\to 0} \frac{1}{\beta} \sum_{i\omega_n} G_{\beta\alpha}(m,n;i\omega_n) \, e^{i\omega_n 0^+} \tag{S47}$$

$$= \frac{1}{2\pi} \int d\omega \, G_{\beta\alpha}(m,n;i\omega) \, e^{i\omega 0^+} \,. \tag{S48}$$

For each spin sector this calculation can be done separately. The total energy difference is then given by

$$\Delta E_{tot} = \Delta E_\uparrow + \Delta E_\downarrow = 2\,\Delta E_\uparrow - J \,. \tag{S49}$$

Since we only need the first few diagonals of the Green functions to evaluate the formula, the inversion scales only linear with the number of unit cells [$\mathcal{O}(N)$]. Therefore, the usage of this method allowed us to simulate much larger systems (with up to $8 \cdot 10^5$ unit cells). Additionally, it was possible to calculate the RKKY coupling for larger distances with smaller J_{RKKY} since the numerical error could be reduced. In Fig. S1 we compare the results obtained with this algorithm with those calculated with ED. We can see that the results for moderate distances perfectly agree. For very large distances we find that the Green functions approach shows even better results than the ED since the numerical error of the ED starts influencing the results.

[1] E. N. Economou, *Green's Functions in Quantum Physics*, third edition (Springer, Berlin, 2006).
[2] N. Müller, D. M. Kennes, J. Klinovaja, D. Loss, and H. Schoeller, Phys. Rev. B **101**, 155417 (2020).
[3] F. Guinea, C. Tejedor, F. Flores, and E. Louis, Phys. Rev. B **28**, 4397 (1983).
[4] M. P. Lopez Sancho, J. M. Lopez Sancho, and J. Rubio, J. Phys. F: Met. Phys. **15**, 851 (1985).
[5] C. H. Lewenkopf and E. R. Mucciolo, Journal of Computational Electronics **12**, 203 (2013).
[6] M. M. Odashima, B. G. Prado, and E. Vernek, Rev. Bras. Ens. Fis. **39**, e1303 (2017).
[7] K. S. Dy, Shi-Yu Wu, and T. Spratlin, Phys. Rev. B **20**, 4237 (1979).
[8] G. Meurant, SIAM J. Matrix Anal. Appl. **13**, 707 (1992).
[9] S. Andergassen, T. Enss, V. Meden, W. Metzner, U. Schollwöck, and K. Schönhammer, Phys. Rev. B **70**, 075102 (2004).

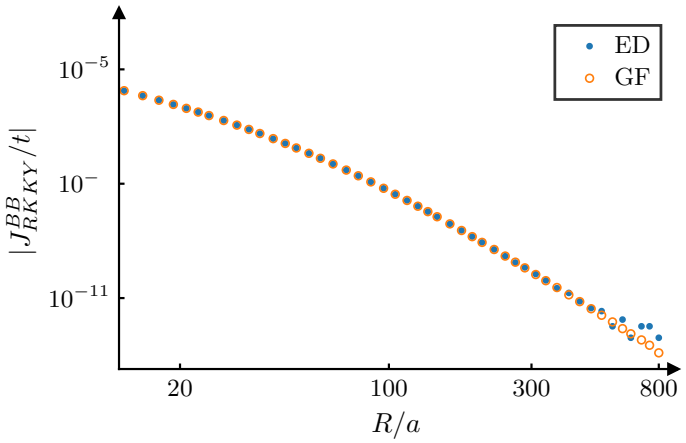

FIG. S1. Comparison of the results obtained by exact diagonalization (ED) and the described Green function approach (GF). We show the absolute value of the RKKY coupling $|J^{BB}_{RKKY}|$ in dependence of the distance R with $J_1 = J_2 = 0.2t$. The results are calculated with a system size of 4000 unit cells but they are converged up to numerical errors. For moderate R we find perfect agreement between the two methods. For very large R we start to see some differences due to the numerical error of the ED. The GF algorithm therefore enables us to calculate the RKKY interaction for larger distances.